sciendo

TATRA MOUNTAINS
Mathematical Publications

DOI: 10.2478/tmmp-2021-0033
Tatra Mt. Math. Publ. **80** (2021), 119–134

IMPROVEMENT AND HANDLING OF THE SEGMENTATION MODEL WITH AN INFLATION TERM

Omondi Polycarp Okock[1,2] — Jozef Urbán[2] — Karol Mikula[1]

[1]Slovak University of Technology, Bratislava, SLOVAKIA

[2]TatraMed Software s.r.o , Bratislava, SLOVAKIA

ABSTRACT. The use of balloon models to address the problems of "snakes" based models was introduced by Laurent D. Cohen. This paper presents a geodesic active contours model with a modified external force term that includes a balloon model. This balloon model makes the segmentation surface to behave like a balloon inflated by the external forces. In this paper, we show an automatic way to control the behaviour of the external force with respect to the segmentation evolution. The external forces, comprised of edge and inflation terms, push the segmentation surface to edges, while curvature regularizes the evolution. As segmentation evolves, the influence of the applied inflation force is determined by how close we are to the edges. With this setup, the initial segmentation does not need to be close to the object's edges, instead it is inflated by the balloon model towards the edges. Closer to the edges, the influence of the inflation force is adjusted accordingly. The force's influence is completely turned off when the evolution is stable (reached the edges), then only the curvature and edge information is used to evolve the segmentation.

This approach solves the issues associated with inclusion of balloon model. These issues are that the inflation force can overpower forces from weak edges, or they can cause the contour to be slightly larger than the actual minima. We present examples of the improved model for segmentation of human bladder images. Weak edges are more prevalent in medical images, and the automated handling of the inflation forces gives promising results for this kind of images.

2010 Mathematics Subject Classification: 65K10, 35Q68, 65Y05, 65Y20.

Keywords: geodesic active contours, balloon model, estimation, curve fitting, curve smoothing.

We thank TatraMed Software s.r.o. for technical support and to ImageInLife for funding - This project has received funding from the European Union's Horizon 2020 research and innovation programme under the Marie Sklodowska-Curie grant agreement No. 721537. The third author was also supported by the grants APVV-19–0460 and VEGA 1/0436/20.

1. Introduction

We introduce a new segmentation model for Geodesic active contours, which significantly improves detection for noisy images. The model was used for automatic segmentation of noisy CT bladder images in 3D. We present the features of this new model with promising experimental results.

Kass et al. [7] developed an active contours segmentation model, and called it the snake model. The snake model is an energy minimizing spline guided by external constraint forces and influenced by image forces that pull it toward features such as lines and edges. The problem of using such active contours is that they do not have the information on how to fill in the gaps in the object or they do not become stationary at the object boundary if the boundary is noisy, blurred or of low contrast. Proposals to address these challenges have been made by researchers including the following. The use of balloon models to address the problems of "snakes" based models was introduced by Laurent D. Cohen [3]. Caselles et al. [2] proposed a segmentation scheme based on relation between active contours and minimal distance curves. Their scheme segments an image by evolving the active contours controlled by a scaling function.

We have defined a level-set based Geodesic active contours model, similar to [10]. The model is placed inside the image, and subject to influence of "external forces" which move and deform it from initial position and drawn to the image edges until it fits the best. We are interested in **improving** the model behaviour, more so when segmenting images with weak edges, noisy or have missing boundary information. To achieve this, we are proposing an automatic approach for managing the model's external forces influence. Usually, this force pushes the model towards the image edges. For images with weak edges or noisy or having missing boundary information, the forces can overpower the weak edges or cause the contour to be slightly larger than the actual minima. We modify it such that the external forces influence is reduced as the model gets closer to the edges and completely turned off when the model reaches the image edges.

The external forces are composed of a balloon model and edge detection terms. Both of these components have been defined from the image data properties. This model presents the following advantages:

- Suitable for segmenting noisy, weak edges images, e.g. medical images.
- Minimal user input needed to fine tune model parameters.
- More stable numerical results.

In the next section, we introduce the model and present its main ideas. We give the experimental results after applying the model to automatic bladder detection from CT pelvis images.

2. Segmentation model with an inflation term

The described general segmentation model is similar to [10]. Let $u(\mathbf{x}, t)$ be the level-set function, where $\mathbf{x}(t) = [x(t), y(t), z(t)]$ denotes the position vector of a surface Γ, at time t. The evolution of $u(\mathbf{x}, t)$ is such that at each time t the surface Γ represents the same isosurface of $u(\mathbf{x}, t)$ as follows

$$u(\mathbf{x}, t) = c, \tag{1}$$

where c is a constant. The total differential of the level-set function becomes

$$\frac{du(\mathbf{x}(t), t)}{dt} = \frac{du(x(t), y(t), z(t), t)}{dt} = 0, \tag{2}$$

$$\frac{\partial u(\mathbf{x}, t)}{\partial t} + \frac{\partial u(\mathbf{x}, t)}{\partial x}\frac{\partial x(t)}{\partial t} + \frac{\partial u(\mathbf{x}, t)}{\partial y}\frac{\partial y(t)}{\partial t} + \frac{\partial u(\mathbf{x}, t)}{\partial z}\frac{\partial z(t)}{\partial t} = 0, \tag{3}$$

which can be rewritten in the form

$$\frac{\partial u(\mathbf{x}, t)}{\partial t} + \frac{d\mathbf{x}(t)}{dt} \cdot \nabla u(\mathbf{x}, t) = 0, \tag{4}$$

$$u(\mathbf{x}, 0) = u^0(\mathbf{x}), \quad \text{for} \quad x \in D,$$

where $u^0(\mathbf{x})$ is an initial condition. Let

$$\mathbf{V}(\mathbf{x}, t) = \frac{d\mathbf{x}(t)}{dt}$$

be the *force term*. Then eq. (4) has the form

$$\frac{\partial u(\mathbf{x}, t)}{\partial t} + \mathbf{V}(\mathbf{x}, t) \cdot \nabla u(\mathbf{x}, t) = 0. \tag{5}$$

The force term controls the evolution of the level-set function. It is composed of the external force and the curvature terms, see Figure 1.

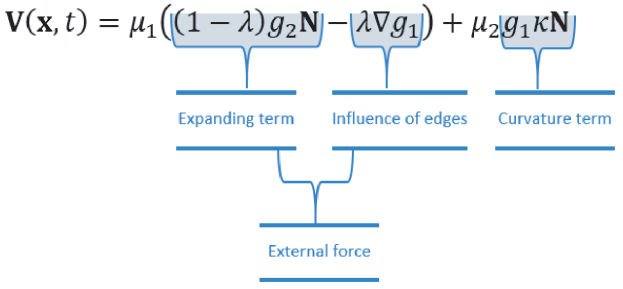

FIGURE 1. The composition of the force terms in the segmentation model.

Similar to [10], it is defined as

$$\mathbf{V}(\mathbf{x},t) = \mu_1\big((1-\lambda)g_2\mathbf{N} - \lambda\nabla g_1\big) + \mu_2 g_1\kappa\mathbf{N}, \tag{6}$$

where μ_1, μ_2 and λ are parameters, $\mathbf{N} = \frac{\nabla u}{|\nabla u|}$ is the outer unit normal vector, $\kappa = -\nabla\cdot\frac{\nabla u}{|\nabla u|}$ is curvature, $g_1 = g_1(|\nabla G_\sigma \star I|) = \frac{1}{1+k_1|\nabla G_\sigma \star I|^2}$ and g_2 defined as

$$g_2 = g_2(I,\rho,k_2) = \frac{1}{1+k_2(I-\rho)^2}. \tag{7}$$

Both g_1 and g_2 are scaling functions, where g_1 is an edge detector function, g_2 is an **inflation term**, with $k_2 > 0$ a parameter, ρ is the average value computed from voxels inside the initial segmentation surface and I is voxel value. Both ρ and I can be a reasonably chosen value, characterizing color, intensity or texture of segmented object in the image.

This model evolves segmentation function towards the image edges, level sets are expanded in normal direction by the inflation term and evolution is regularized by curvature. Since there is an inflation force, if the edge is too weak, the segmentation function can pass through this edge if it is singularity with the rest of the surface being inflated. The regularization effect with the help of inflation force then removes discontinuity created at that point and segmentation function passes through the curve.

3. Discretization of the model

The full form of eq. (5) is

$$u_t + \left(\mu_1\big((1-\lambda)g_2\frac{\nabla u}{|\nabla u|} - \lambda\nabla g_1\big)\right)\cdot\nabla u - \mu_2 g_1\nabla\cdot\left(\frac{\nabla u}{|\nabla u|}\right)\frac{\nabla u}{|\nabla u|}\cdot\nabla u = 0, \tag{8}$$

and simplified to

$$u_t + \mu_1\nu\cdot\nabla u - \mu_2 g_1|\nabla u|\nabla\cdot\left(\frac{\nabla u}{|\nabla u|}\right) = 0, \tag{9}$$

where $\nu = (1-\lambda)g_2\dfrac{\nabla u}{|\nabla u|} - \lambda\nabla g_1$.

3.1. Time discretization

In order to discretize eq. (9) in time, we apply the semi-implicit approach that guarantees unconditional stability with respect to the diffusion term. Let us suppose that the equation in time interval $I = [0,T]$ and in N equal time steps. The time step is denoted as $\tau = \frac{T}{N}$. The time discretization is then as follows

$$\frac{u^{n+1}-u^n}{\tau} + \mu_1\nu^n\cdot\nabla u^n - \mu_2 g_1|\nabla u^n|\nabla\cdot\left(\frac{\nabla u^{n+1}}{|\nabla u^n|}\right) = 0. \tag{10}$$

3.2. Space discretization

To discretize eq. (10) in space, we apply the so-called flux-based level set finite volume [6] method. Consider the product rule as follows

$$\nabla \cdot (u^n \nu^n) = u^n \nabla \cdot \nu^n + \nu^n \nabla \cdot u^n,$$

we can express $\nu^n \cdot \nabla u^n = \nabla \cdot (u^n \nu^n) - u^n \nabla \cdot \nu^n$ and replace in eq. (10). We integrate eq. (10) over a finite volume p

$$\int_p \frac{u^{n+1}-u^n}{\tau} dx + \mu_1 \int_p \nabla \cdot (u^n \nu^n)\, dx - \mu_1 \int_p u^n \nabla \cdot \nu^n dx - \mu_2 \int_p g_1 |\nabla u^n| \nabla \cdot \left(\frac{\nabla u^{n+1}}{|\nabla u^n|} \right) dx. \tag{11}$$

Integrating

$$\int_p \frac{u^{n+1} - u^n}{\tau}\, dx$$

becomes

$$\int_p \frac{u^{n+1} - u^n}{\tau} dx = m(p) \frac{u_p^{n+1} - u_p^n}{\tau}, \tag{12}$$

where $m(p)$ is the measure of finite volume p.

For the advection part,

$$\mu_1 \int_p \nabla \cdot (u^n \nu^n)\, dx - \mu_1 \int_p u^n \nabla \cdot \nu^n dx,$$

we use divergence theorem in both terms and constant representation of solution in finite volume p in the second term, we obtain

$$\approx \mu_1 \int_{\partial p} (u^n \nu^n) \cdot \mathbf{n}_{\partial p} dS - \mu_1 u_p^n \int_{\partial p} \nu^n \cdot \mathbf{n}_{\partial p} dS. \tag{13}$$

Using integral fluxes [6, 8, 9], we define inflows and outflows through the voxel sides as

$$\nu_{pq}^{in} = \min\left(\nu_{pq}^n, 0\right), \qquad \nu_{pq}^{out} = \max\left(\nu_{pq}^n, 0\right),$$

where ν_{pq}^n is define as

$$\begin{aligned} \nu_{pq}^n &= \int_{\partial p} \nu^n \cdot \mathbf{n}_{\partial p} dS \\ &= \int_{e_{pq}} (1-\lambda) g_2 \frac{\nabla u^n}{|\nabla u^n|} - \lambda \nabla g_1 \cdot \mathbf{n}_{\partial p} dS \\ &\approx \frac{m(e_{pq})}{m(\sigma_{pq})} \left[(1-\lambda) g_2 \frac{u_q^n - u_p^n}{|\nabla\, u_{pq}^n|} - \lambda \nabla g_1 \right], \end{aligned} \tag{14}$$

where e_{pq} denotes the edge between finite volumes p and q, $\mathbf{n}_{\partial p}$ is the normal vector to e_{pq} from p to q, $m(e_{pq})$ is the measure of edge between finite volumes p and q, and $m(\sigma_{pq})$ denotes the measure of line between centres of finite volumes p and q.

We define an approximate gradient ∇g_1 in the finite volume p using central differences [9]

$$\nabla g_{1_p} = (G_{pe}, G_{pn}, G_{pt}) = (-G_{pw}, -G_{ps}, -G_{pb}),$$

where

$$\begin{aligned} -G_{pw} &= G_{pe} \approx \frac{g_e - g_w}{2h}, \\ -G_{ps} &= G_{pn} \approx \frac{g_n - g_s}{2h}, \\ -G_{pb} &= G_{pt} \approx \frac{g_t - g_b}{2h}, \end{aligned}$$

h is the edge size and g_q is the neighbouring cell value of the g_p such that $q \in N_p$. For g_2 function, we approximate the average of neighbouring points as follows

$$g_2 = \frac{g_{2_p} + g_{2_q}}{2}.$$

Substituting these in eq. (15), we get ν^n_{pq} defined as

$$\nu^n_{pq} = \frac{m(e_{pq})}{m(\sigma_{pq})} \left[(1-\lambda) \frac{g_{2_p} + g_{2_q}}{2} \frac{u^n_q - u^n_p}{|\nabla u^n_{pq}|} - \lambda G_{pq} \right]. \tag{15}$$

We can then approximate eq. (13) by using upwind principle as in [6,9] to obtain the following

$$\begin{aligned} \mu_1 \int_{\partial p} (u^n \nu) \cdot \mathbf{n}_{\partial p} dS - \mu_1 u^n_p \int_{\partial p} \nu \cdot \mathbf{n}_{\partial p} dS \approx \\ \mu_1 \sum_{q \in N_p} \nu^{in}_{pq} u^n_q + \mu_1 \sum_{q \in N_p} \nu^{out}_{pq} u^n_p - \mu_1 \sum_{q \in N_p} \nu^{in}_{pq} u^n_p - \mu_1 \sum_{q \in N_p} \nu^{out}_{pq} u^n_p = \\ \mu_1 \sum_{q \in N_p} \nu^{in}_{pq} \left(u^n_q - u^n_p \right), \end{aligned} \tag{16}$$

where N_p is an index set containing all the neighbouring finite volumes q to p.

For discretization of the diffusion term, we consider $|\nabla u_n|$ as a constant on finite volume p to become $|\nabla u^n_p|$. Then we apply the divergence theorem, approximating the derivative, $\nabla u^{n+1} \approx \frac{u^{n+1}_q - u^{n+1}_p}{m(\sigma_{pq})}$ and $|\nabla u^n|$ on the edges, denoted as $|\nabla u^n_{pq}|$ using the diamond cell scheme [4,8]. This is similar to approximating

the mean curvature term as done in [5]

$$\mu_2 \int_p g_1 |\nabla u^n| \nabla \cdot \left(\frac{\nabla u^{n+1}}{|\nabla u^n|} \right) dx \approx \mu_2 g_1 |\nabla u_p^n| \sum_{q \in N_p} \frac{m(e_{pq})}{m(\sigma_{pq})} \frac{u_q^{n+1} - u_p^{n+1}}{|\nabla u_{pq}^n|}. \quad (17)$$

Combining eq. (12), (16), (17), we can obtain discrete form of (11) and making u_p^n the subject as

$$\begin{aligned} u_p^n = u_p^{n+1} &+ \mu_1 \frac{\tau}{m(p)} \sum_{q \in N_p} \nu_{pq}^{in} \left(u_q^n - u_p^n \right) \\ &- \mu_2 \frac{\tau}{m(p)} g_1 |\nabla u_p^n| \sum_{q \in N_p} \frac{m(e_{pq})}{m(\sigma_{pq})} \frac{u_q^{n+1} - u_p^{n+1}}{|\nabla u_{pq}^n|}. \end{aligned} \quad (18)$$

The solution of eq. (18) is then obtained by using Gaus-Seidel iterative method. For boundary values, we impose the Neumann boundary condition.

4. Improving the model behaviour

For images with weak or missing edge information or noisy images, the inflation force from the proposed model can overpower the weak forces, see [3]. We have proposed to regulate the influence of this term. When the segmentation function is far away from the edge, we inflate it towards the edge using the inflation force. As it gets closer to the edges, we propose to reduce the influence of the inflation and use the edge forces to evolve the segmentation. And finally, when the segmentation function has reached the edge (stable), we turn off the influence completely and we use the edge forces and curvature terms. To regulate the inflation term, g_2, we modified eq. (6) by adding two more parameters η and ζ as shown in eq. (19). In this way, we can control influence of edges and inflation term independently. g_2 influence is regulated by varying ζ.

$$\mu_1 \big((1 - \lambda) \zeta \, g_2 \mathbf{N} - \eta \lambda \nabla g_1 \big). \quad (19)$$

For monitoring the segmentation evolution, we calculate the L2-norm difference between current and previous segmentation. The goal is to find the specific iteration to reduce or turn off g_2. Our proposal will use curve's extrema information to determine the iterations. It is difficult to determine the extrema of the curve of the differences between current u_p^{n+1} and previous u_p^n segmentation's while the segmentation is still running. To solve this, we built an estimate function that estimates the next ϖ differences from the currently calculated difference values. We refer to ϖ as the offset value. The estimation starts only after the number of iterations during the segmentation process is greater than ϖ.

Let y be a discrete curve of values calculated from L^2-norm of the difference between u_p^{n+1} and u_p^n at each iteration n. It is defined as follows

$$y^{n+1} = \frac{1}{N}\sum_{p=1}^{N}\left(u_p^{n+1} - u_p^n\right)^2, \tag{20}$$

where N is the total number of points in their level set presentation. The y curve values are noisy as seen in Figures 5, 6, 7 and 8. To remove this noise, we perform *curve fitting* by constructing a smoothing function to approximately fit the data. Let y_{smooth} be the curve fitted by applying moving average of order m as follows

$$y_{\text{smooth}}^n = \frac{1}{m}\sum_{i=-k}^{k} y^{n+i}, \tag{21}$$

where $m = 2k + 1$.

The smoothed curve will be used as an input to the estimating function instead of the original noisy curve data. In addition, the smooth curve will help in capturing the curve's extrema. We also define a function, y_{diff} as follows

$$y_{\text{diff}}^n = y_{\text{smooth}}^{n+1} - y_{\text{smooth}}^n. \tag{22}$$

With the above definitions, we define function to estimate, denoted as y_{est}.

$$\begin{aligned} d_{\text{diff\_smooth}}^n &= \frac{1}{\xi}\sum_{i=-k}^{k} y_{\text{diff}}^{n+i}, \\ y_{\text{est}}^n &= y_{\text{smooth}}^n + \varpi d_{\text{diff\_smooth}}^n. \end{aligned} \tag{23}$$

We have set $\xi = 2k + 1$ and ϖ is the offset. For our setup, we used $k = 2$ or $\xi = 5$.

With the above setup, we find the first iteration n to turn off g_2, such that y_{est}^n becomes non-positive. The estimate corresponds to the global minima of the estimated curve. The advantage of this approach is that we don't have to wait for the segmentation process to finish then determine the global minima from the calculated values.

After determining what iteration to turn off g_2, we try to determine the iteration to automatically reduce its influence. From early experiments, see Figures 5, 6, 7 and 8, we observed our initial choice was approximately close to the curve's global maximum. From our experience, the global maximum is not the best measure for choosing the iteration to reduce the influence. This is because

in some experiments, this can be in the first early steps, which we found too early to reduce or turn off g_2 influence. Instead, we have chosen to base the iteration to reduce the influence on the mid-area of the curve y.

The $n + \varpi$ estimated values are copied from y_{est} to y. Then we use the *Trapezoid rule* [1] to calculate the area under the new curve. Then we calculate the mid-area and find the closest iteration to this mid-area. At this iteration, we set to reduce g_2 influence. In the next subsection, we show results from applying the novel automatic approach to handle g_2.

5. Numerical experiments

In our experimental setup, we tested on noisy synthetic bladder images. The exact dimensions for each bladder image was $100 \times 100 \times 40$ voxels. We created artificial noisy bladder images by adding varying high level of noise to the exact images. We chose salt and pepper where 75 % and 85 % of the images were affected with the noise. From our experiments with different types of noise and associating levels, *salt and pepper* noise levels $>=$ 75 % segmentation failed. In the Figures 2, 3, 4, are the artificial bladder images with 75 % and 85 % noise levels slice views. In our setup, we used a set of 3 bladders.

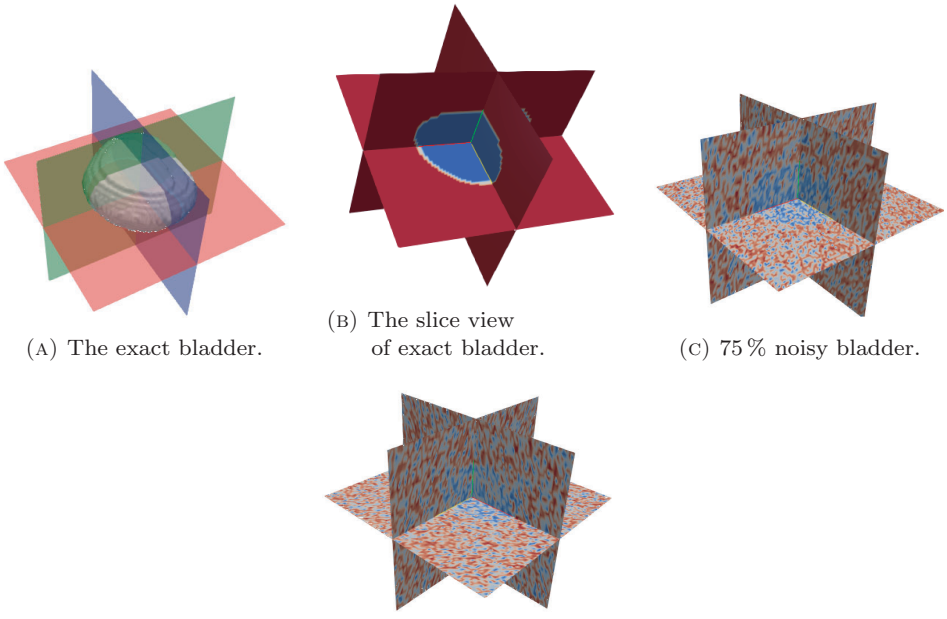

(A) The exact bladder.

(B) The slice view of exact bladder.

(C) 75 % noisy bladder.

(D) 85 % noisy bladder.

FIGURE 2. The first bladder image.

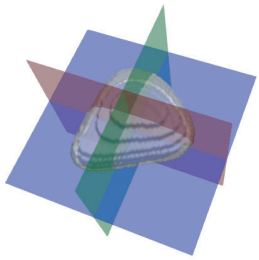

(A) The exact bladder.

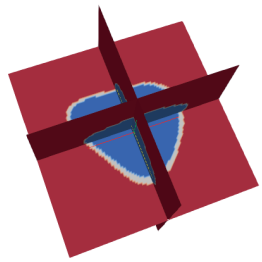

(B) The slice view of exact bladder.

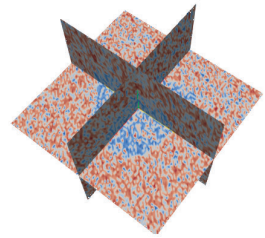

(C) 75 % noisy bladder.

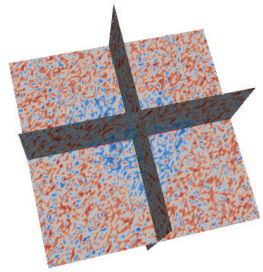

(D) 85 % noisy bladder.

FIGURE 3. The second bladder image.

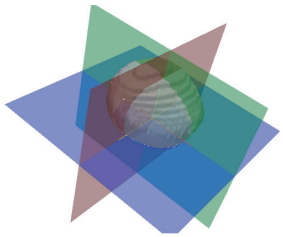

(A) The exact bladder.

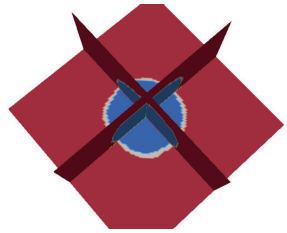

(B) The slice view of exact bladder.

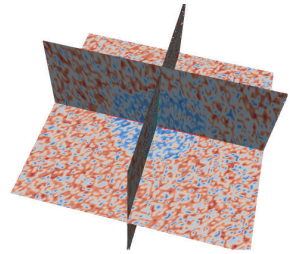

(C) 75 % noisy bladder.

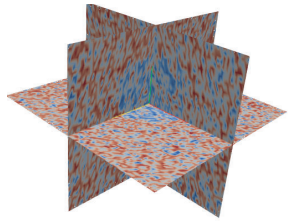

(D) 85 % noisy bladder.

FIGURE 4. The third bladder image.

Since we also had the precise bladder region of interest, ROI, we were able to test how well the segmentation performed by comparing the final results with the precise data. At 75 % noise level, we made the following observations for segmentation, summarized in the Table 1. The error values are the L^2-norm of difference between the final segmentation and the exact results.

TABLE 1. L^2-norm after segmenting 75 % noisy images.

Bladder	1	2	3
L^2-norm	16.8316	10.0207	0.63506

In addition, we calculated the L^2-norm of difference between the current, u_p^{n+1} and previous segmentation, u_p^n. These results are shown in Figure 5. From Table 1, L^2-norm results, bladder 1 & 2 segmentation were not successful when compared to patient 3.

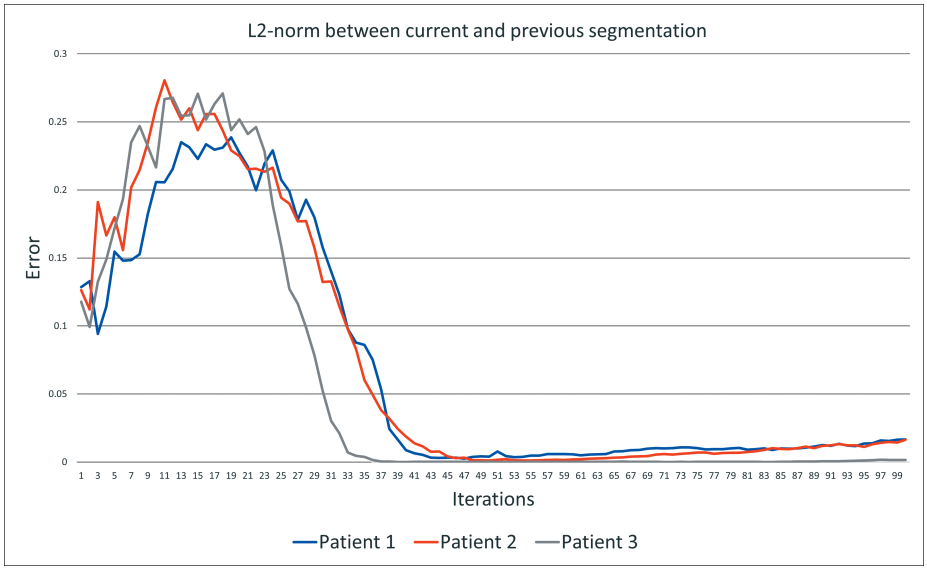

FIGURE 5. L^2-norm between current and previous segmentation at 75 % noise level.

5.1. Results of manual selections of reduce and turn off steps for g_2 function

Before applying the proposed approach to automatically handle the inflation term, we manually first identified the iteration before the segmentation results overflowed the exact result, see Table 2.

TABLE 2. Selected iterations to turn off g_2.

Bladder	1	2	3
Iteration	20	15	11

From our observation, these chosen numbers of iterations were close to the curves' maxima (see Figure 5). At these iterations, g_2 influence was turned off (setting $\lambda = 1$). The results after this attempt are shown in Table 3 and Figure 6. Comparing the results in Table 1 versus 3 and Figure 5 versus 6, there was a significant improvement in the first approach to improve and build on the g_2 function.

TABLE 3. L^2-norm after segmenting 75 % noisy images.

Bladder	1	2	3
L^2-norm	0.4147	0.5200	0.0724

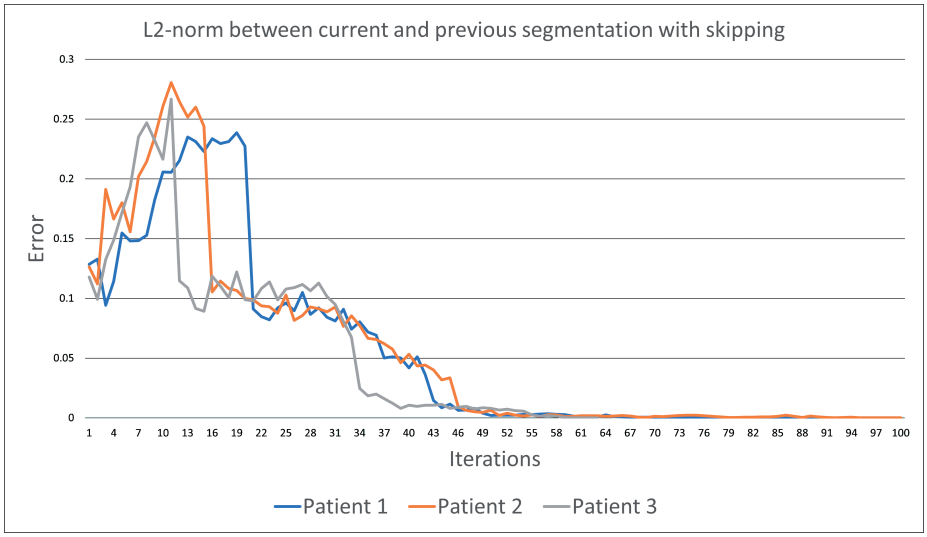

FIGURE 6. L^2-norm between current and previous segmentation at 75 % noise level after skipping g_2 at selected iterations.

We proceeded to test the same approach on the 85 % noisy images. The segmentation results are shown in Table 4 and Figure 7. We also observe segmentation failing to segment the bladders. As before, we identified the iteration just before the segmentation overflowed the exact shape. Segmentation is assumed

to have reached equilibrium if it is not changing (evolving). This can be interpreted when the difference from the previous segmentation is approximately *zero*. As a result, we also identified the iteration with L^2-norm closest to the minima of the three curves.

TABLE 4. L^2-norm after segmenting 85 % noisy images.

Bladder	1	2	3
L^2-norm	36.7712	67.3418	45.0444

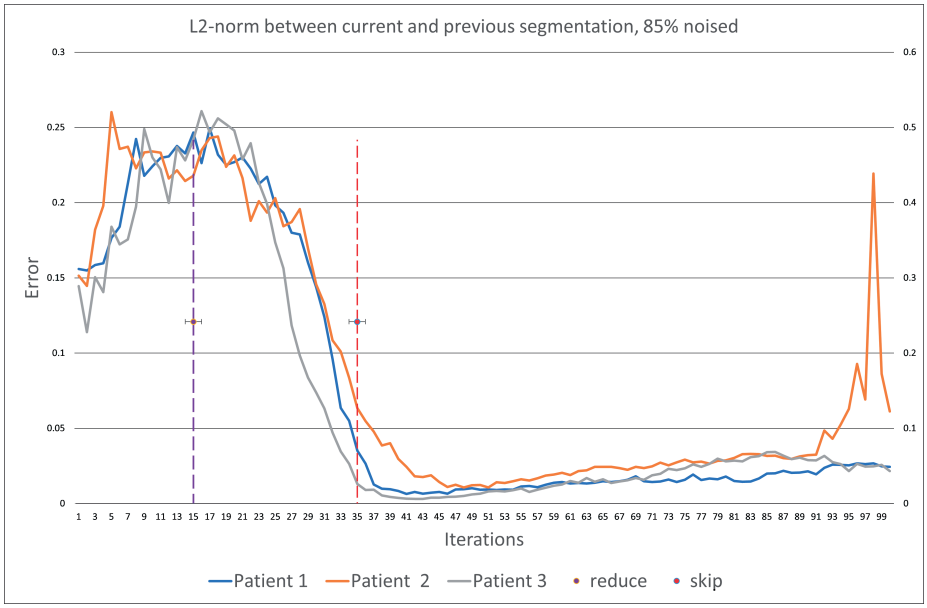

FIGURE 7. L^2-norm between current and previous segmentation at 85 % noise level. Vertical lines represent the iteration to reduce or turn off g_2 influence.

In the second approach, we want to reduce g_2 gradually by 50 % then turn it off completely at the iteration closest to their minima's. To simplify the process, we set the same iterations for the three bladders, i.e. in iteration 15 g_2 influence is reduced and from iteration 35 onward it's skipped. They are represented by the vertical lines in Figure 7.

The results after applying the above mentioned modifications are summarized in Table 5 and Figure 8. Compared to the results in Table 4, there were significant improvements observed in all the datasets. From these results, reducing or skipping of g_2 has a significant improvement on the segmentation results.

TABLE 5. L^2-norm after segmenting 85 % noisy images with both reduction and skipping of g_2.

Bladder	1	2	3
L^2-norm	1.1380	6.2533	0.2299

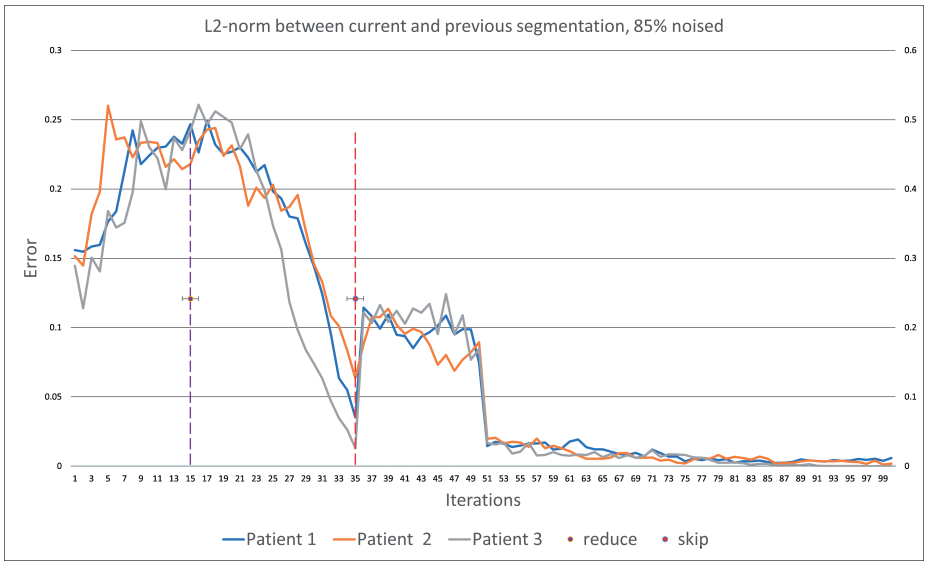

FIGURE 8. L^2-norm between current and previous segmentation at 85 % noise level with both reduction and skipping of g_2.

In real data problems, the exact object to be segmented is rarely known in advance and so our two first approaches of setting the iterations to reduce or turn off g_2 by checking for overflow are not realistic for a real solution. In addition, determining a curve's extrema is not possible if the segmentation is still running. With the mentioned limitations, we apply our proposed approach in the next section.

5.2. Results of automatic selections of reduce and turn off steps for g_2 function

In this section, we present the results for the automatically selected iterations for skipping and skipping g_2 influence. In Table 6, we show the found values versus our hand-picked values in our original attempt for the 85 % noisy images.

TABLE 6. Comparison of manual versus automatic selection of iterations to reduce and turn off g_2 influence.

(A) Manually selected iterations.

Bladder	1	2	3
Reduce iteration	15	15	15
Turn off iteration	35	35	35

(B) Automatically calculated iterations.

Bladder	1	2	3
Reduce iteration	15	15	14
Turn off iteration	37	38	32

In Table 5, we showed results after our manual set iterations to reduce and skip. In Table 7, we show new results of segmentation with the automatic handling of g_2. In the setup, after the first estimated zero has been found and mid-area determined, the segmentation process is restarted automatically from the initial iteration. Once the segmentation process reaches the found iterations, automatic reduction and skipping of g_2 is applied without any user intervention.

TABLE 7. Comparison of segmentation L^2-norm results for 85 % noisy image between manual and automatic handling of g_2.

(A) Iterations set manually.

Bladder	1	2	3
L^2-norm	1.1380	6.2533	0.2299

(B) Iterations calculated automatically.

Bladder	1	2	3
L^2-norm	1.2245	5.2651	0.1906

6. Conclusion

We presented a level-set based Geodesic active contours model that solves some of the problems encountered when balloon models are introduced to 'active models'. We modified the definition and behaviour of the external force, specifically the inflation term. We automatically controlled its influence on the segmentation during the evolution. This was based on a simple estimation algorithm to estimate differences of the current and previous segmentation to determine at what iteration to change the inflation term influence.

We presented promising experiment 3D results, showing the advantages of the approach, specifically for very noisy images. The challenge with finding the correct set of parameters for segmentation have been made simpler by the proposed approach to automatically handle the inflation term influence.

REFERENCES

[1] ATKINSON, K.: *An Introduction to Numerical Analysis*, 2 edition, John Wiley & Sons, Inc. New York, 1989.

[2] CASELLES, V.—KIMMEL, R.—SAPIRO, G.: *Geodesic active contours*, Internat. J. Comput. Vision **22** (1997), no. 1, 61–79.

[3] COHEN, L. D.: *On active contour models and balloons*, CVGIP: Image Understanding **53** (1991), no. 2, 211–218.

[4] DRBLÍKOVÁ, O.—MIKULA, K.: *Semi-implicit diamond-cell finite volume scheme for 3D nonlinear tensor diffusion in coherence enhancing image filtering* (Robert Eymard et al. eds.) In: Proceedings of the 5th International Symposium, Aussois, June, 2008, *Finite Volumes for Complex Applications Vol. V: Problems and Perspectives* ISTE and WILEY, London, 2008, pp. 343–350.

[5] EYMARD, R.—HANDLOVIČOVÁ, A.—MIKULA, K.: *Study of a finite volume scheme for the regularized mean curvature flow level set equation*, IMA J. Numer. Anal. **31** (2011), no. 3, 813–846.

[6] FROLKOVIČ, P.—MIKULA, K.: *Flux-based level set method: A finite volume method for evolving interfaces*, Appl. Numer. Math. **57** (2007), no. 4, 436–454.

[7] KASS, M.—WITKIN, A.—TERZOPOULOS, D.: *Snakes: Active contour models*, Internat. J. Comput. Vision **1** (1988), 321–331.

[8] MIKULA, K.—REMEŠÍKOVÁ, M.: *Finite volume schemes for the generalized subjective surface equation in image segmentation*, Kybernetika, **45** (2009), no. 4, 646—656.

[9] MIKULA, K.—SMÍŠEK, M.—ŠPIR, V.: *Parallel algorithms for segmentation of cellular structures in 2D+time and 3D morphogenesis data*. In: Proceedings of the Conference Algoritmy, Vol. 2012, pp. 416–426.

[10] URBÁN, J.: *The new improvements of Atlas based image segmentation*, Slovak University of Technology in Bratislava, Reg. no.: SvF-10911-38875 (2016), 47–50.

Received November 8, 2020

Omondi Polycarp Okock
Karol Mikula
Department of Math. and Descriptive Geometry
Faculty of Civil Engineering
Slovak University of Technology
Radlinského 11
810 05 Bratislava
SLOVAKIA
E-mail: polycarp.okock@stuba.sk
karol.mikula@stuba.sk

Omondi Polycarp Okock
Jozef Urbán
TatraMed Software s.r.o
Líščie údolie 9
841 04 Bratislava
SLOVAKIA
E-mail: polycarp.okock@tatramed.sk
jozef.urban@tatramed.sk